AIAA SciTech Forum
6-10 January 2020, Orlando, FL
AIAA Scitech 2020 Forum

10.2514/6.2020-0787

High Efficiency Integrated Propeller-CoFlow Jet Airfoil in Cruise

Yan Ren * Gecheng Zha †
Coral Gables, FL 33124
Dept. of Mechanical and Aerospace Engineering
University of Miami, Coral Gables, Florida 33124

Abstract

This paper presents the study of propeller-CoFlow Jet (CFJ) active flow control airfoil in cruise flight. The propeller-CFJ system is an integrated system with propellers mounted above the CFJ wing suction surface. Differing from the conventional configurations that separate the propeller and the airfoil, the propeller-CFJ system is designed together to enhance cruise efficiency via interaction between the CFJ and the propeller. The propeller pulls more flow toward the airfoil suction surface and the CFJ take advantage of the flow to achieve better aerodynamic performance. The simulations employ 3D RANS solver with Spalart-Allmaras (S-A) turbulence model, 3rd order WENO scheme for the inviscid fluxes, and 2nd order central differencing for the viscous terms.

The aerodynamic performance, energy expenditure, and flow field are compared between airfoils with and without CFJ/propeller, including different propeller strength. The 2D simulation results show that the cruise efficiency is increased by 46.86% for case with CFJ only, and by 20.62% for case with propeller only compare to the baseline airfoil with no flow control. However, for the cases with both the CFJ and the actuator, the cruise efficiency improvement can be even larger due to the interaction of the CFJ and the actuator. The parametric study on the actuator strength shows that the cruise efficiency gains are around 80% for all cases and have a tenancy of increase with the increase of the propeller strength. The 3D full aircraft simulations show that the aerodynamic efficiency increases 7.11% and the productivity efficiency increases 11.17% with the help of the propeller actuator.

Nomenclature

CFJ	Co-flow jet
AoA	Angle of attack
LE	Leading Edge
TE	Trailing Edge
S	Planform area
s	Wing Span length
c	Profile chord
U	Flow velocity
q	Dynamic pressure $0.5\,\rho\,U^2$
p	Static pressure

* Postdoc Researcher, Ph.D., AIAA member
† Professor, AIAA Associate Fellow, Professor of the University of Miami

ρ	Air density
$\dot{m}$	Mass flow
M	Mach number
P	Pumping power
∞	Free stream conditions
C_L	Lift coefficient $L/(q_\infty S)$
C_D	Drag coefficient $D/(q_\infty S)$
T_C	Propeller actuator thrust coefficient
C_μ	Jet momentum coef. $\dot{m}_j U_j/(q_\infty S)$
P_c	CFJ power coefficient $L/(q_\infty S V_\infty)$
P_{PC}	Propeller actuator power coefficient

1 Introduction

The lift and thrust generation of conventional aircraft in cruise flight are separated, as the lift is produced by the airfoil while the trust is produced by the propeller actuator. However, the actuator wake is an energetic region that could be utilized by the airfoil. With the help of the novel Co-Flow Jet (CFJ) flow control method developed recently [1, 2, 3, 4, 5, 6, 7, 8, 9, 10, 11], the propeller actuator and the CFJ airfoil can be integrated as a high efficiency system in cruise condition.

In this work, a propeller-CoFlow Jet (CFJ) active flow control system is proposed and studied for cruise flight. The propeller-CFJ system is an integrated system with propellers mounted above the CFJ wing suction surface as shown in Fig. 1. The mechanism is that the propeller pulls more flow toward the airfoil suction surface. It accelerate the flow more and increase the circulation. At the same time, the CFJ benefits from the suction effect of the propeller downstream of the injection slot with reduced power required for CFJ. It results in an increase of the cruise efficiency for the integrated system. The system is designed together to enhance cruise efficiency via interaction between the CFJ and the propeller. Simulations are conducted to investigate the effect of such interaction, and the effect of actuator strength.

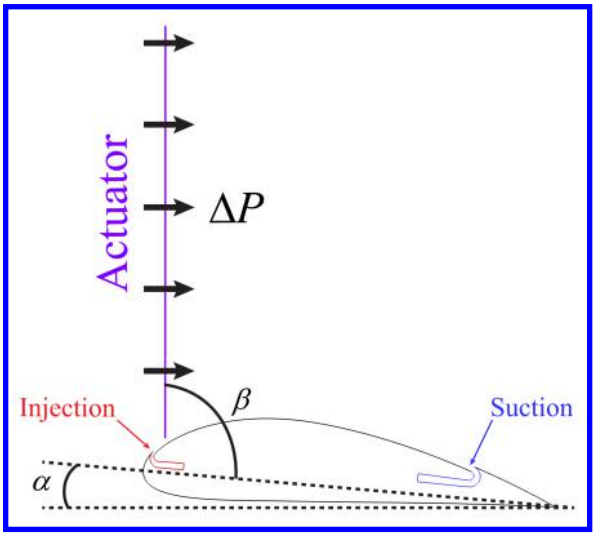

Figure 1: Schematic plot of a typical propeller-CFJ airfoil.

2 The Co-Flow Jet Airfoil

The CFJ airfoil has an injection slot near the leading edge(LE) and a suction slot near the trailing edge(TE) on the airfoil suction surface as sketched in Fig. 2. A small amount of mass flow is withdrawn into the airfoil near the TE, pressurized and energized by a micro-compressor system inside the airfoil, and then injected near the LE in the direction tangent to the main flow. The whole process does not add any mass flow to the system and hence is a zero-net mass-flux flow control.

The CFJ airfoil flow control mechanism achieves a radical lift augmentation, drag reduction and stall margin increase at a very low energy expenditure. It can not only achieve ultra-high maximum lift coefficient, but also significantly enhance cruise productivity efficiency and cruise wing loading from subsonic to transonic conditions[12, 13, 14, 15, 16, 17]. Yang and Zha [16] discovered in 2017 that a CFJ airfoil can achieve Super-Lift Coefficient(SLC), which is a lift coefficient that exceeds the theoretical limit of potential flow developed by Smith[18] and is defined below:

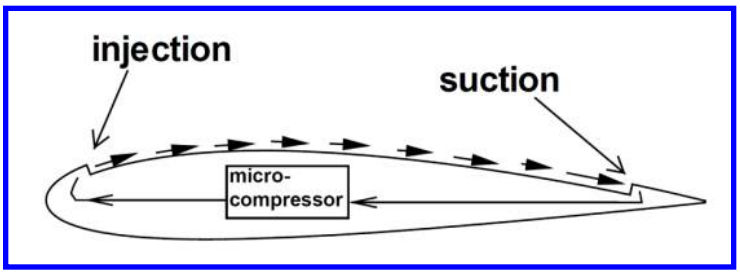

Figure 2: Baseline airfoil and CFJ Airfoil.

$$C_{Lmax} = 2\pi(1 + \frac{t}{c}) \tag{1}$$

The focus of this paper is to continue to improve the cruise efficiency via the integrated propeller- CFJ airfoil system. Most of the active flow control methods are aimed at suppressing flow separation, delaying airfoil stall angle of attack (AoA), and increasing the maximum lift coefficient. Few active flow controls are able to increase cruise efficiency when the flow control energy consumption is included to the system. This is because conventional airfoils usually cruise at their optimal efficiency point at a low angle of attack with very benign flow conditions. The CFJ airfoil provides the potential to increase cruise efficiency[8, 12, 13, 15, 19, 20].

3 CFJ Parameters

The following are the parameters used to define the CFJ airfoil performance.

3.1 Lift and Drag Calculation

The momentum and pressure at the injection and suction slots produce a reactionary force, which is automatically measured by the force balance in wind tunnel testing. However, for CFD simulation, the full reactionary force needs to be included. Using control volume analysis, the reactionary force can be calculated using the flow parameters at the injection and suction slot opening surfaces. Zha et al. [2] give the following formulations to

calculate the lift and drag due to the jet reactionary force for a CFJ airfoil. By considering the effects of injection and suction jets on the CFJ airfoil, the expressions for these reactionary forces are given as :

$$F_{x_{cfj}} = (\dot{m}_j V_{j1} + p_{j1} A_{j1}) * cos(\theta_1 - \alpha) - (\dot{m}_j V_{j2} + p_{j2} A_{j2}) * cos(\theta_2 + \alpha) \tag{2}$$

$$F_{y_{cfj}} = (\dot{m}_{j1} V_{j1} + p_{j1} A_{j1}) * sin(\theta_1 - \alpha) + (\dot{m}_{j2} V_{j2} + p_{j2} A_{j2}) * sin(\theta_2 + \alpha) \tag{3}$$

where the subscripts 1 and 2 stand for the injection and suction respectively, and θ_1 and θ_2 are the angles between the injection and suction slot's surface and a line normal to the airfoil chord. α is the angle of attack.

The total lift and drag on the airfoil can then be expressed as:

$$D = R'_x - F_{x_{cfj}} \tag{4}$$

$$L = R'_y - F_{y_{cfj}} \tag{5}$$

where R'_x and R'_y are the surface integral of pressure and shear stress in x (drag) and y (lift) direction excluding the internal ducts of injection and suction. For CFJ wing simulations, the total lift and drag are calculated by integrating Eqs.(4) and (5) in the spanwise direction.

3.2 Jet Momentum Coefficient

The jet momentum coefficient C_μ is a parameter used to quantify the jet intensity. It is defined as:

$$C_\mu = \frac{\dot{m} V_j}{\frac{1}{2}\rho_\infty {V_\infty}^2 S} \tag{6}$$

where $\dot{m}$ is the injection mass flow, V_j is the mass-averaged injection velocity, ρ_∞ and V_∞ denote the free stream density and velocity, and S is the planform area.

3.3 Power Coefficient

CFJ is implemented by mounting a pumping system inside the wing that withdraws air from the suction slot and blows it into the injection slot. The power consumption is determined by the jet mass flow and total enthalpy change as the following:

$$P_{CFJ} = \dot{m}(H_{t1} - H_{t2}) \tag{7}$$

where H_{t1} and H_{t2} are the mass-averaged total enthalpy in the injection cavity and suction cavity respectively, P is the Power required by the pump and $\dot{m}$ the jet mass flow rate. Introducing P_{t1} and P_{t2} the mass-averaged total pressure in the injection and suction cavity respectively, the pump efficiency η, and the total pressure ratio of the pump $\Gamma = \frac{P_{t1}}{P_{t2}}$, the power consumption is expressed as:

$$P_{CFJ} = \frac{\dot{m} C_p T_{t2}}{\eta} (\Gamma^{\frac{\gamma-1}{\gamma}} - 1) \tag{8}$$

where γ is the specific heat ratio equal to 1.4 for air. The power coefficient for CFJ is expressed as:

$$P_c = \frac{P_{CFJ}}{\frac{1}{2}\rho_\infty V_\infty^3 S} \tag{9}$$

The power coefficient for the propeller actuator is:

$$P_{PC} = \frac{T V_\infty}{\frac{1}{2}\rho_\infty S V_\infty^3} = \frac{T}{\frac{1}{2}\rho_\infty S V_\infty^2} = T_C \tag{10}$$

where T is the propeller thrust force; T_C is the propeller thrust coefficient.

For 2D single airfoil simulations, a predetermined extra drag coefficient ($C_{D,P}$) is introduced to the efficiency calculation as the reserve for the 3D induced drag as well as the fuselage drag of an aircraft in real cruise condition. $C_{D,P} = C_{D,I} + C_{D,F}$, where $C_{D,I}$ and $C_{D,F}$ are the induced drag and fuselage drag coefficients, respectively. For 3D full aircraft simulations, the drag of the wing and fuselage are directly calculated. The total drag coefficient ($C_{D,T}$) in 2D and 3D simulations are defined as:

$$2D : C_{D,T} = C_D + C_{D,P} \tag{11}$$

$$3D : C_{D,T} = C_D + C_{D,F} \tag{12}$$

where C_D is the drag coefficient of the wing. For simulations with propeller actuators, the $C_{D,P}$ is given at the start of the simulation, and the actuator strength is iterated during the simulation steps to have the T_C balance with the $C_{D,T}$, which insures the cruise flight condition. For 2D simulations without propeller actuators, the $C_{D,P}$ can be any given values for the ease of comparison of the aerodynamic efficiency.

In order to compare the aerodynamic efficiency of a propeller-CFJ airfoil with that of a conventional airfoil, a corrected aerodynamic efficiency $(C_L/C_{D,T})_c$ is introduced. It takes into consideration of the power needed for the CFJ[8] as well as the power needed for the actuator:

$$(\frac{C_L}{C_{D,T}})_c = \frac{C_L}{C_{D,T} + P_c} = \frac{C_L}{T_C + P_c} = \frac{C_L}{P_{PC} + P_c} \tag{13}$$

where C_L, $C_{D,T}$ and P_c are the total lift coefficient, total drag coefficient, and CFJ pumping power coefficient. The $(C_L/C_{D,T})_c$ incorporates the CFJ power consumed into the drag of the system and the propeller power consumption.

Yang and Zha [16] introduce an airplane productivity concept defined as the airplane gross weight multiplied by their maximum range. To compare the aircraft with the same ratio of initial weight to final weight, the only factor affecting their productivity parameter is C_L^2/C_D. The parameter C_L^2/C_D is hence named productivity efficiency[16]. The productivity efficiency is considered as a more comprehensive parameter than the conventional aerodynamic efficiency C_L/C_D to measure the merit of an airplane aerodynamic design for cruise performance.

The former includes not only the information of C_L/C_D, but also the information of the aircraft weight represented by C_L.

For a propeller-CFJ airfoil system, the productivity efficiency should include the CFJ power consumption and is defined as below:

$$(\frac{C_L^2}{C_{D,T}})_c = \frac{C_L^2}{C_{D,T} + P_c} = \frac{C_L^2}{T_C + P_c} = \frac{C_L^2}{P_{PC} + P_c} \tag{14}$$

For CFJ airfoil, the minimum CFJ pumping power occurs at a fairly high AoA [7, 8]. With the augmentation of CFJ, the subsonic cruise lift coefficient of a CFJ airfoil is usually substantially higher than the conventional airfoil with about the same $(C_L/C_{D,T})_c$ [13]. Such a high lift coefficient is unattainable for conventional airfoil since they would be either stalled or near stalled with very high drag. Hence for CFJ aircraft design, the productivity efficiency $(C_L^2/C_{D,T})_c = C_L(C_L/C_{D,T})_c$ is more informative to be used to reflect the aerodynamic performance.

3.4 CFD Simulation Setup

The in house FASIP (Flow-Acoustics-Structure Interaction Package) CFD code is used to conduct the numerical simulation. The 2D/3D Reynolds averaged Navier-Stokes equation with the one equation Spalart-Allmaras turbulence model are solved. A 3rd order WENO scheme for the inviscid flux [21, 22, 23, 24, 25, 26] and a 2nd order central differencing for the viscous terms [21, 25] are employed to discretize the Navier-Stokes equations. The low diffusion E-CUSP scheme used as the approximate Riemann solver suggested by Zha et al [22] is utilized with the WENO scheme to evaluate the inviscid fluxes. Implicit time marching method using Gauss-Seidel line relaxation is used to achieve a fast convergence rate [27]. Parallel computing is implemented to save wall clock simulation time [28].

3.5 Boundary Conditions

The 3rd order accuracy no slip condition is enforced on the solid surface with the wall treatment suggested in [29] to achieve the flux conservation on the wall. The computational mesh for 2D cases is shown in Fig. 3. Total pressure, total temperature and flow angles are specified at the injection duct inlet, as well as the upstream portion of the far field. Constant static pressure is applied at the suction duct outlet as well as the downstream portion of the far field. The total mesh size is 77,600 for all 2D cases, split into 31 blocks for the parallel computation. For 3D full aircraft simulations, the total mesh size is about 6,000,000, split into 174 blocks for the parallel computation. The far field boundary is about 60 chords away from the airfoil to ensure an accurate simulation. The first grid point on the wing surface is placed at $y^+ \approx 1$. The propeller is simulated using an actuator disk boundary condition with a pressure jump (ΔP) imposed. The pressure jump is given as a percentage of the pressure upstream of the actuator, typically is fairly small and rarely greater than 2%. The pressure jump condition can be very well handled by the Riemann solver employed in the FASIP CFD code.

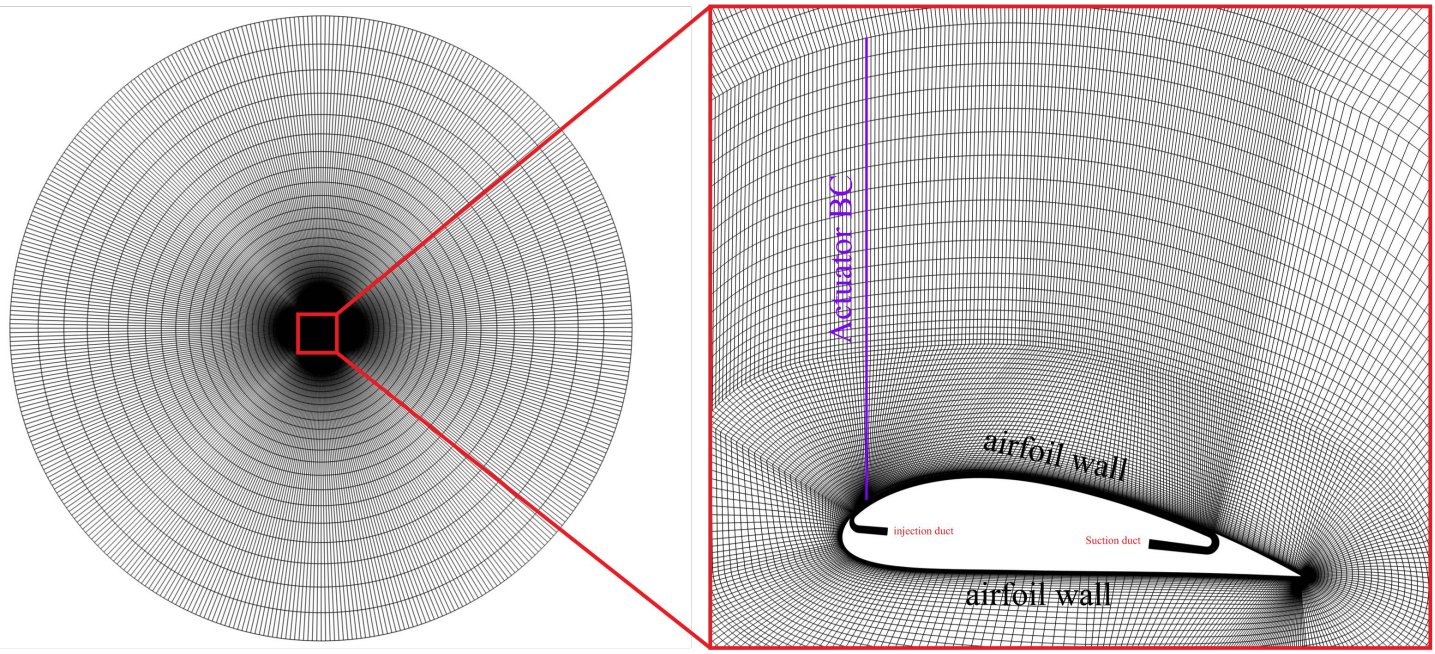

Figure 3: Computational mesh used in the current work.

4 Results and Discussion

In this section, the effect of propeller actuator on CFJ airfoils are presented. Ten cases are discussed here as listed in Table 1, including three 2D baseline cases (B1 - B3), five 2D cases with different $C_{D,P}$ (C1 - C5), and two 3D full aircraft cases (C6 and C7) with and without propeller actuator for comparison. In Table 1, for the usage of CFJ and propeller actuator, 0 means no usage and 1 means it is used. The free stream Mach number for all cases are 0.15 and the Reynolds number is 1,340,000. The airfoil angle of attacks (α angles) are 5° for the cruise condition [8, 10, 11, 12, 13, 19, 20]. The propeller actuator normal to the free stream. The actuator locates near the airfoil leading edge, downstream of of the injection slot and above the suction surface. This configuration is optimized to have maximum cruise efficiency. For the cases with the actuator, the actuator strength, which is quantified by the pressure jump across the actuator ΔP, is iterated during the simulation to have the T_C balanced with the $C_{D,T}$ for the cruise flight condition. All the airfoils used in the present study are CFJ-NACA-6421.

4.1 Cruise Performance of CFJ Airfoils with Acutator

In this section, the cruise performance of the propeller-CFJ airfoils are investigated. Four cases (C2, B1, B2, and B3) are studied here. Case C2 has both CFJ and actuator. Case B1 is the baseline case without CFJ and actuator, case B2 only has the CFJ and case B3 only has the actuator. The C_μ and $C_{D,P}$ are 0.03 and 0.05, respectively. The $C_{D,P}$ value is estimated via 3D full aircraft simulations (C6 and C7).

Table 1: Simulation parameters used in the current work.

Cases	CFJ	Actuator	AR	$Mach$	ΔP	C_μ	$C_{D,P}$
B1	0	0	∞	0.15	N/A	N/A	N/A
B2	1	0	∞	0.15	N/A	0.03	N/A
B3	0	1	∞	0.15	0.113%	N/A	0.05
C1	1	1	∞	0.15	0.055%	0.03	0.025
C2	1	1	∞	0.15	0.089%	0.03	0.05
C3	1	1	∞	0.15	0.123%	0.03	0.075
C4	1	1	∞	0.15	0.157%	0.03	0.1
C5	1	1	∞	0.15	0.191%	0.03	0.125
C6	1	1	20	0.15	0.099%	0.03	N/A
C7	1	0	20	0.15	N/A	0.03	N/A

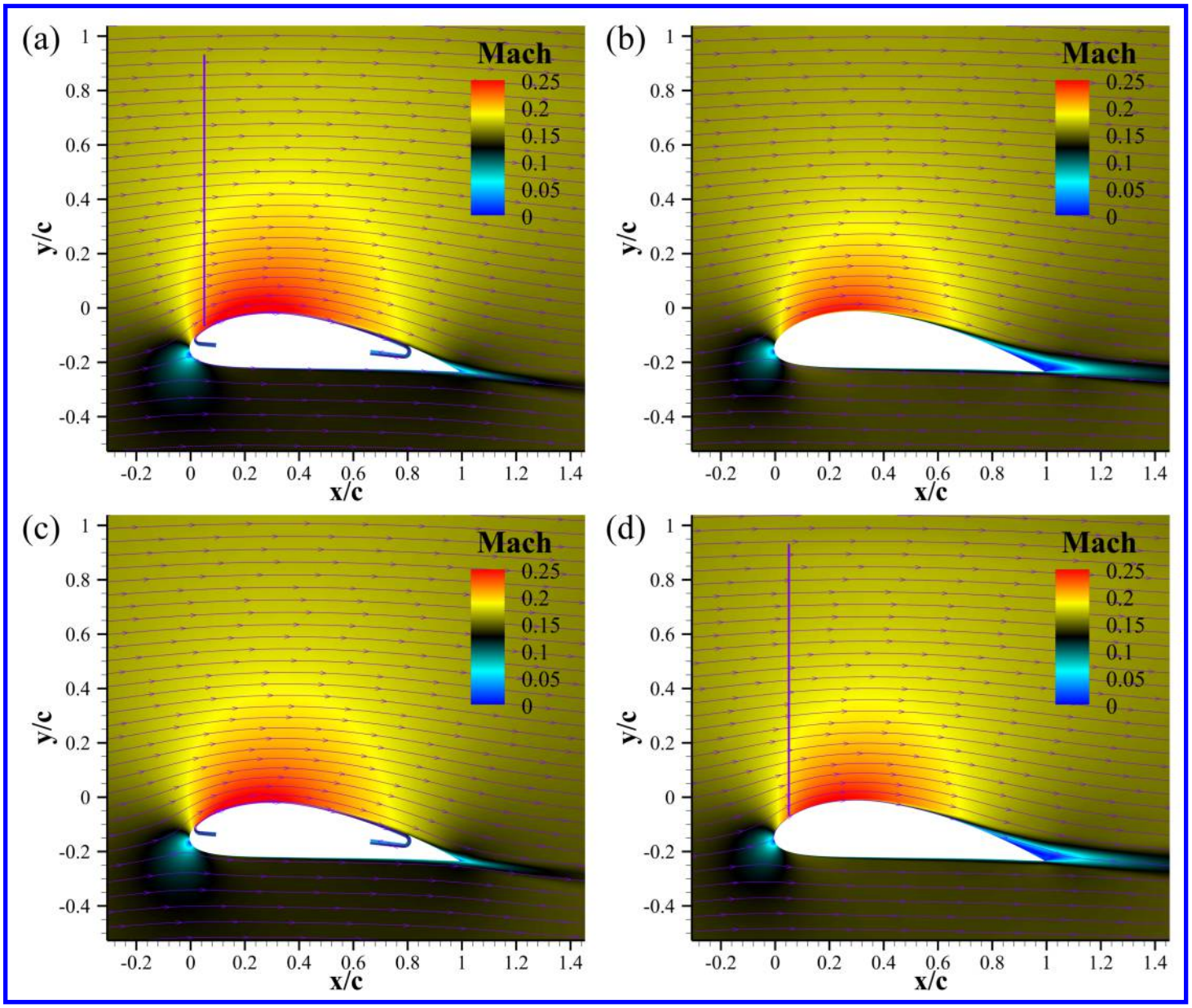

Figure 4: Mach contours and streamlines of (a) case C2, (b) case B1, (c) case B2, and (d) case B3.

Fig. 4 shows the Mach contours and streamlines of those cases. The actuators in case C2 and B3 are marked as purple lines. Cases with CFJ (Fig. 4 a and c) show well attached flow around the airfoil while those without CFJ (Fig. 4 b and d) have a minor flow separation at the trailing edge. The CFJ energize the boundary layer above the suction surface and can make the flow stay attached to very high angle of attack, virtually stall free [16]. On the other hand, the cases with the actuator (Fig. 4 a and d) show larger high speed flow region on the airfoil suction surface. The actuator pulls more flow and accelerate the flow above the airfoil suction surface. The enlarged high speed region is more significant for the CFJ airfoil than the baseline airfoil, indicating that the interaction between the propeller actuator and the CFJ airfoil generates more benefit than the baseline airfoil.

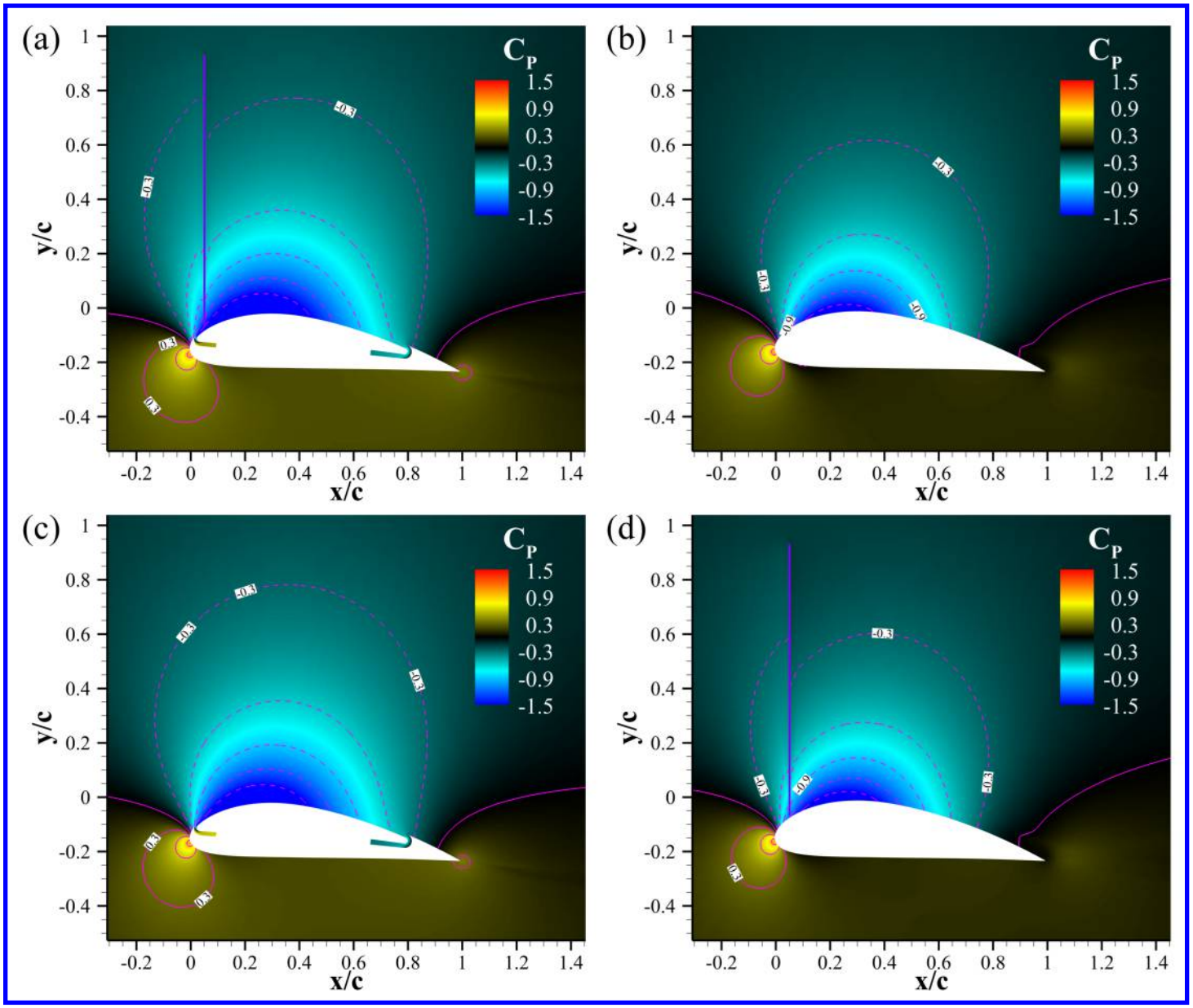

Figure 5: C_P contours of (a) case C2, (b) case B1, (c) case B2 and (d) case B3.

Fig. 5 shows the C_P contours of the four cases. The actuator model introduces static pressure discontinuity that can be observed in Fig. 5 (a) and (d). Compare case C2 and B2, the existence of actuator result in greater

lower pressure region on the suction surface. Similar results can be identified in case B1 and B3. For cases with CFJ, it is clear to see that the low pressure region on the suction surface is enhanced (Fig. 5 a and c). It will lead to larger lift generation for the cases with CFJ since the pressure difference between the airfoil pressure and suction surface is increased.

Table 2 lists the aerodynamic performance of the four cases. Also listed are the $(C_L/C_{D,T})_c$ gains in percentage compared with the baseline case B1.

For the force production, case C2, which has both the CFJ and the actuator, presents the largest lift, while the drag even turns negative (thrust generation). The CFJ only case (case B2) also shows much greater lift and much smaller drag compared with the baseline case. The actuator only case (B3) shows moderate improvement of the lift enhancement and drag reduction. Overall, the usage of CFJ greatly improves the lift increase and drag reduction of the airfoil.

For the aerodynamic efficiency shown in Table 2, the CFJ only and actuator only case both show improvement with the CFJ one being substantially greater. The gains are around 46.86% and 20.62%, respectively. For the case with both CFJ and actuator, the $(C_L/C_{D,T})_c$ is 24.07, which is the largest efficiency improvement of 77.9%. It is clear that the interaction of CFJ and actuator improves the most for the overall performance of the airfoil. Comparing the productivity efficiency between Case C2 and B1, the improvement is 150%.

Table 2: Aerodynamic performance of case C2, B1, B2 and B3.

Cases	C_L	C_D	$C_{D,P}$	$C_{D,T}$	P_c	P_{PC}	$(C_L/C_{D,T})_c$	$(C_L^2/C_{D,T})_c$	$\Delta(C_L/C_{D,T})_c$
C2	1.395	-0.0016	0.05	0.0484	0.0096	0.0484	24.07	33.56	77.90%
B1 (baseline)	0.989	0.0231	0.05	0.0731	0	N/A	13.53	13.38	0.0%
B2	1.342	0.0082	0.05	0.0582	0.01	N/A	19.65	26.38	46.86%
B3	1.042	0.0138	0.05	0.0638	0	0.0638	16.32	17.00	20.62%

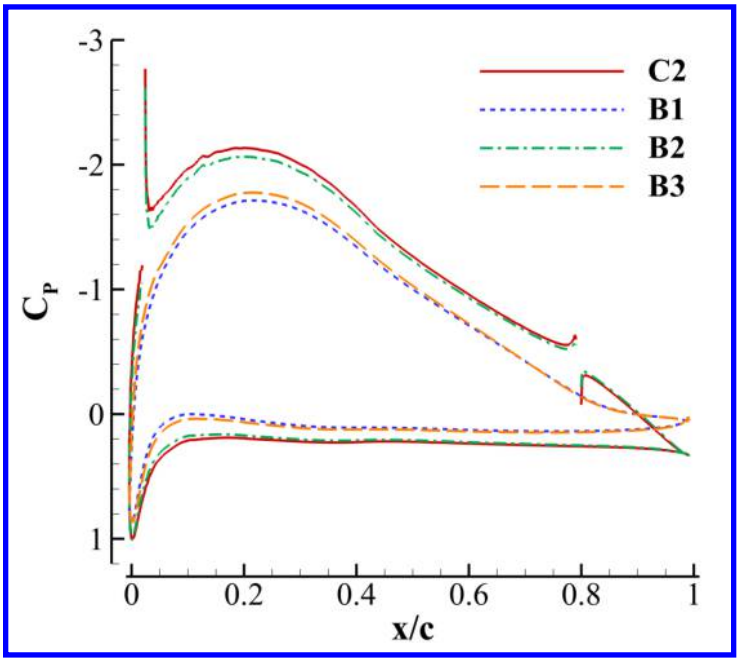

Figure 6: C_P distributions on the airfoil surface of case C2, B1, B2 and B3.

The pressure coefficient distributions on the CFJ airfoil surfaces are shown in Fig. 6. The discontinuity of the curves are due to the injection and suction slots of the CFJ airfoils. From the plot we can see that the cases with CFJ show much lower pressure in suction surface and much higher pressure in pressure surface (red and green curves). The actuator can further reduce the pressure in most part of the airfoil suction surface, while it can increase the pressure near the leading edge at the pressure surface.

4.2 Effect of Actuator Strength

This section investigate the propeller actuator strength effect on the cruise performance of the propeller-CFJ airfoils system. Five cases (C1 - C5) are studied here, with the $C_{D,P}$ gradually increases (from 0.025 to 0.125). The actuator strength in terms of ΔP increases accordingly to generate enough thrust to overcome the larger extra drag. The C_μ of all theses cases remain constant at 0.03.

Table 3 lists the aerodynamic performance of the five cases. Also listed are the $(C_L/C_{D,T})_c$ gains in percentage compared with the baseline case B1. Note that the $(C_L/C_{D,T})_c$ of case B1 are calculated according to the different extra drag coefficient $C_{D,P}$ from case C1 to C5.

We can see from table 3 that the lift coefficient gradually increases with the ΔP, while the drag coefficient decreases with the ΔP. The drag of the airfoil turns negative when the ΔP increased to 0.089% (case C2), which means thrust generation. The P_c of the CFJ also drops a little bit when ΔP increases. The aerodynamic efficiency in terms of $(C_L/C_{D,T})_c$ drops as the ΔP increases since the prescribed extra drag is increased. However, the efficiency gains for all cases are around 80% and have a trend of improving with the ΔP.

Table 3: Aerodynamic performance with varying propeller actuator strength.

Cases	C_L	C_D	$C_{D,P}$	$C_{D,T}$	P_c	P_{PC}	ΔP	$(C_L/C_{D,T})_c$	$(C_L^2/C_{D,T})_c$	$\Delta(C_L/C_{D,T})_c$
C1	1.376	0.0024	0.025	0.0274	0.0098	0.0274	0.055%	36.99	50.88	79.95%
C2	1.395	-0.0016	0.05	0.0484	0.0096	0.0484	0.089%	24.07	33.56	77.90%
C3	1.413	-0.0057	0.075	0.0693	0.0093	0.0693	0.123%	17.97	25.38	78.21%
C4	1.433	-0.0097	0.1	0.0903	0.0091	0.0903	0.157%	14.42	20.65	79.47%
C5	1.450	-0.0139	0.125	0.1111	0.0089	0.1111	0.191%	12.08	17.51	80.87%
B1	0.989	0.0231	0.025	0.0481	0	N/A	N/A	20.56	20.33	0.0%
			0.05	0.0731				13.53	13.38	
			0.075	0.0981				10.08	9.97	
			0.1	0.1231				8.03	7.95	
			0.125	0.1481				6.68	6.60	

4.3 Cruise Performance of Full Aircraft with Propeller-CFJ Wing

In this section, cruise performance of 3D full body aircraft with propeller-CFJ wing is investigated. The aircraft configuration is modified from the electric airplane designed by Lefebvre and Zha [12] with the vertical and horizontal tail removed for simplicity. The aspect ratio is 21.3 and the cruise Mach number is 0.15. The propeller effect is simulated as a rectangle actuator disk to mimic multiple propellers distributed along the wing span. Two cases (C6 and C7) are studied with case C6 having a propeller actuator above the wing suction surface. The propeller strength in terms of ΔP is iterated during the simulation to generate T_C to balance the total drag coefficient $C_{D,T}$.

Fig. 7 shows the Mach contours of flow field slices along the wing span for the two cases. It shows that the high speed area decreases from the wing root to the wing tip for both cases due to loading decrease. The Mach contours in case C6 show discontinuity due to the existence of the propeller actuator. In addition, the high Mach number zone in case C6 is larger than that of case C7. The actuator pulls more flow to the wing suction surface and interact with the CFJ to accelerate the flow above the wing suction surface. The advantage seen in the 2D also exists in the 3D wing fuselage configuration, but the magnitude is substantially reduced. One interesting observation is that the wake is more energized by the propeller with a high speed trail from the tip of the propeller.

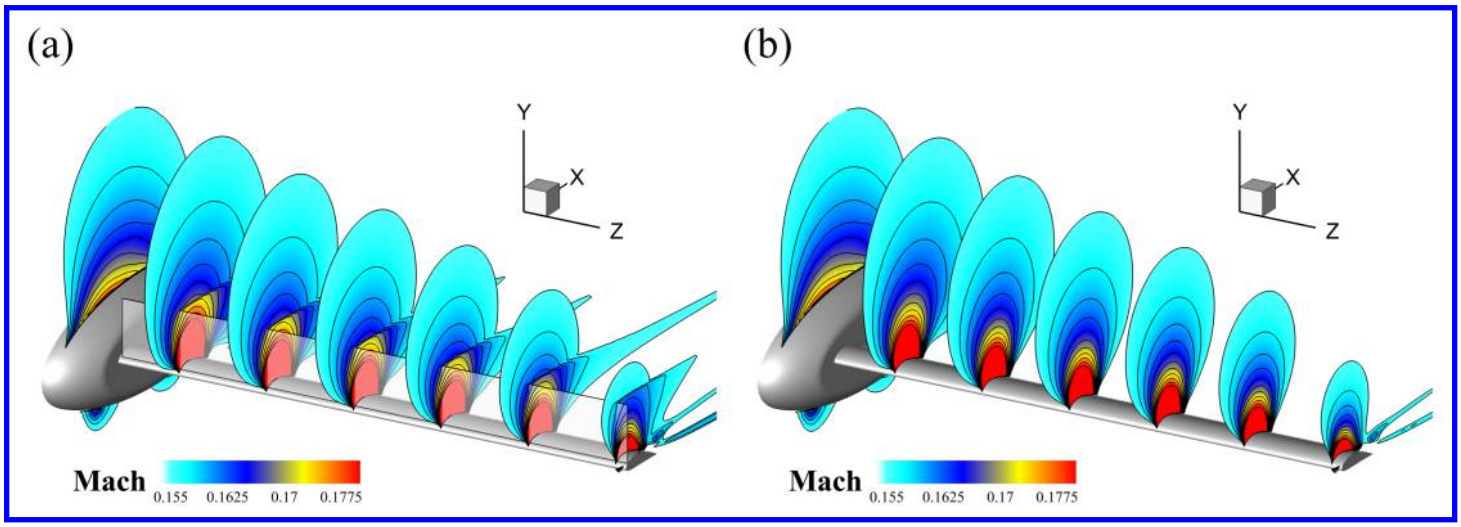

Figure 7: Mach contour of flow field slices along the wing span for (a) case C6 and (b) case C7.

Fig. 8 shows the C_P contours on the aircraft surface for the two cases. The C_P distribution on the fuselage surface are almost identical for the two cases except for a small part near the wing root, which shows a larger low pressure region for case C6. It leads to slightly better aerodynamic performance of the fuselage. The low pressure region on the wing suction surface for case C6 is a little larger compared with that of the case C7.

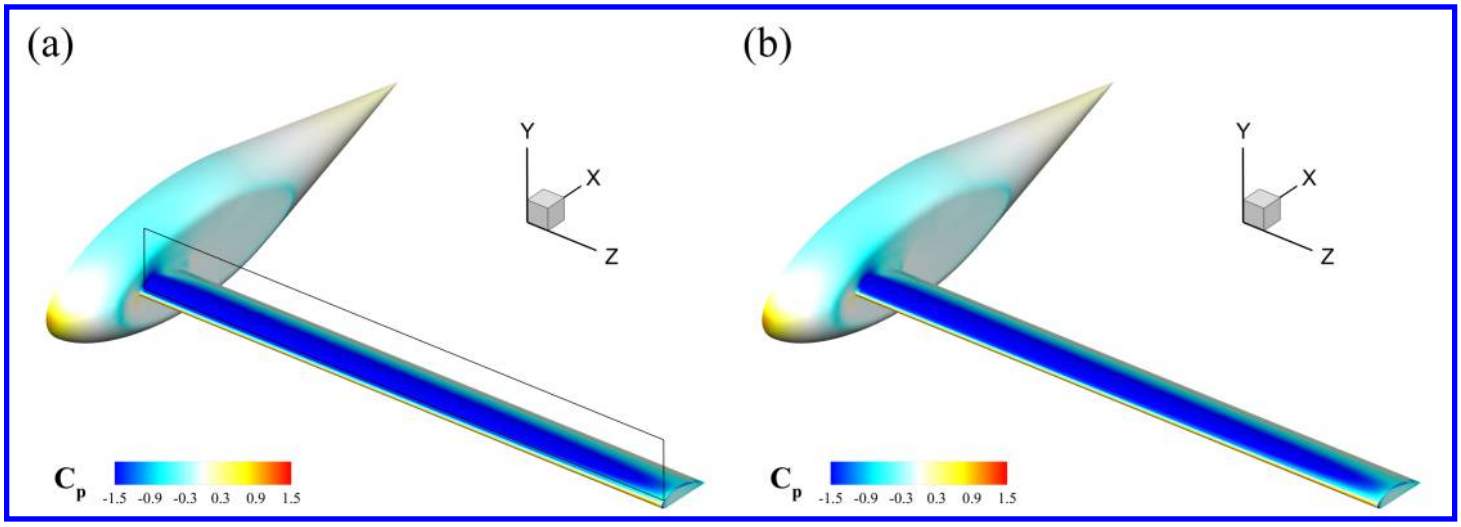

Figure 8: C_P contours on the aircraft surface of (a) case C6 and (b) case C7.

Table 4 lists the aerodynamic performance of the two cases. Comparing the case C6 to the case C7, Table 4

Table 4: Aerodynamic performance of case C2, B1, B2 and B3.

Cases	Items	C_L	C_D	$C_{D,T}$	P_c	P_{PC}	ΔP	$(C_L/C_{D,T})_c$	$(C_L^2/C_{D,T})_c$
C6	Wing	1.202	0.0394	0.0491	0.0150	0.0491	0.099%	19.89	25.28
	Fuselage	0.0681	0.0097						
	Total	1.270	0.0491						
C7	Wing	1.154	0.0405	0.0507	0.0157	N/A	N/A	18.57	22.74
	Fuselage	0.0673	0.0103						
	Total	1.221	0.0507						

indicates that the C_L of the wing increases 4.16%, the C_D of the wing decreases 2.72%. For the fuselage, the C_L increases 1.19% and the C_D decreases 5.83%. In addition, the CFJ power coefficient P_c decreases 4.46%. The aerodynamic efficiency in terms of $(C_L/C_{D,T})_c$ increases 7.11% and the productivity efficiency in terms of $(C_L^2/C_{D,T})_c$ increases 11.17%. Clearly, the propeller-CFJ wing still brings a significant advantage over the CFJ wing only, but in a substantially less amount than the 2D case. The reason appears to be the higher lift coefficient also creating higher induced drag, which offsets the large benefit shown in the 2D cases. How to preserve the large benefit gain of CFJ airfoil from 2D to 3D is a challenging problem. The simulation to compare the propeller-CFJ wing system with the baseline wing system is in progress.

5 Conclusion

This paper investigate the advantages of the integrated propeller-CFJ airfoil system. Both 2D and 3D simulations are presented to evaluate the aerodynamic performance of the propeller-CFJ system. The 2D simulation results show that the cruise efficiency is increased by 46.86% for case with CFJ only, and by 20.62% for case with actuator only compared with the baseline airfoil with no flow control. The 2D case with both CFJ and propeller shows 77.9% of the aerodynamic efficiency improvement. The 2D trade study on varying the actuator strength shows that the cruise efficiency gains are about 80% for all the cases. The 3D full aircraft simulations show that the aerodynamic efficiency of the propeller-CFJ system is increased by 7.11% compared with the CFJ wing only system. The productivity efficiency increases 11.17%. The advantage shown in 2D by the propeller-CFJ system is offset significantly in 3D by the induced drag.

6 Acknowledgment

The CFD simulations are conducted on Pegasus supercomputing system at the Center for Computational Sciences at the University of Miami.

Disclosure: Dr. GeCheng Zha is on the Board of Directors/Corporate officer for CoFlow Jet and holds equity in CoFlow Jet. Dr. Zha is also the inventor of intellectual property licensed to CoFlow Jet.

References

[1] G.-C. Zha and D. C. Paxton, "A Novel Flow Control Method for Airfoil Performance Enhancement Using Co-Flow Jet." *Applications of Circulation Control Technologies*, Chapter 10, p. 293-314, Vol. 214, Progress in

Astronautics and Aeronautics, AIAA Book Series, Editors: Joslin, R. D. and Jones, G.S., 2006.

[2] G.-C. Zha, W. Gao, and C. Paxton, "Jet Effects on Co-Flow Jet Airfoil Performance," *AIAA Journal, No. 6,*, vol. 45, pp. 1222–1231, 2007.

[3] G.-C. Zha, C. Paxton, A. Conley, A. Wells, and B. Carroll, "Effect of Injection Slot Size on High Performance Co-Flow Jet Airfoil," *AIAA Journal of Aircraft*, vol. 43, 2006.

[4] G.-C. Zha, B. Carroll, C. Paxton, A. Conley, and A. Wells, "High Performance Airfoil with Co-Flow Jet Flow Control," *AIAA Journal*, vol. 45, 2007.

[5] Wang, B.-Y. and Haddoukessouni, B. and Levy, J. and Zha, G.-C., "Numerical Investigations of Injection Slot Size Effect on the Performance of Co-Flow Jet Airfoil," *Journal of Aircraft*, vol. Vol. 45, No. 6,, pp. pp.2084–2091, 2008.

[6] B. P. E. Dano, D. Kirk, and G.-C. Zha, "Experimental Investigation of Jet Mixing Mechanism of Co- Flow Jet Airfoil." AIAA-2010-4421, 5th AIAA Flow Control Conference, Chicago, IL, 28 Jun - 1 Jul 2010.

[7] B. P. E. Dano, G.-C. Zha, and M. Castillo, "Experimental Study of Co-Flow Jet Airfoil Performance Enhancement Using Micro Discreet Jets." AIAA Paper 2011-0941, 49th AIAA Aerospace Sciences Meeting, Orlando, FL, 4-7 January 2011.

[8] A. Lefebvre, B. Dano, W. Bartow, M. Fronzo, and G. Zha, "Performance and energy expenditure of coflow jet airfoil with variation of mach number," *Journal of Aircraft*, vol. 53, no. 6, pp. 1757–1767, 2016.

[9] A. Lefebvre, G-C. Zha, "Numerical Simulation of Pitching Airfoil Performance Enhancement Using Co-Flow Jet Flow Control," *AIAA paper 2013-2517*, June 2013.

[10] A. Lefebvre, G-C. Zha, "Cow-Flow Jet Airfoil Trade Study Part I : Energy Consumption and Aerodynamic Performance," *32nd AIAA Applied Aerodynamics Conference, AIAA AVIATION Forum, AIAA 2014-2682*, June 2014.

[11] A. Lefebvre, G-C. Zha, "Cow-Flow Jet Airfoil Trade Study Part II : Moment and Drag," *32nd AIAA Applied Aerodynamics Conference, AIAA AVIATION Forum, AIAA 2014-2683*, June 2014.

[12] Lefebvre, A. and Zha, G.-C. , "Design of High Wing Loading Compact Electric Airplane Utilizing Co-Flow Jet Flow Control." AIAA Paper 2015-0772, AIAA SciTech2015: 53nd Aerospace Sciences Meeting, Kissimmee, FL, 5-9 Jan 2015.

[13] Lefebvre, A. and Zha, G.-C., "Trade Study of 3D Co-Flow Jet Wing for Cruise and Takeoff/Landing Performance." AIAA Paper 2016-0570, AIAA SCITECH2016, AIAA Aerospace Science Meeting, San Diego, CA, 4-8 January 2016.

[14] Lefebvre, A. and Dano, B. and Bartow, W. and Di Franzo, M. and Zha, G.-C., "Performance Enhancement and Energy Expenditure of Co-Flow Jet Airfoil with Variation of Mach Number." AIAA Paper 2013-0490, AIAA Journal of Aircraft, DOI: 10.2514/1.C033113, 2016.

[15] Liu, Z.-X. and Zha, G.-C., "Transonic Airfoil Performance Enhancement Using Co-Flow Jet Active Flow Control." AIAA Paper 2016-3472, AIAA AVIATION 2016, 8th AIAA Flow Control Conference, Washington, D.C, June 13-17, 2016.

[16] Yang, Y.-C. and Zha, G.-C., "Super-Lift Coefficient of Active Flow Control Airfoil: What Is the Limit?." AIAA Paper 2017-1693, AIAA SCITECH2017, 55th AIAA Aerospace Science Meeting, Grapevine, Texas, 9-13 January 2017.

[17] G.-C. Zha, Y.-C. Yang, Y. Ren, and B. McBreen, "Super-lift and thrusting airfoil of coflow jet-actuated by micro-compressors." AIAA Paper 2017-3061, AIAA AVIATION 2018, Atlanta, GA , 25 - 29 June 2018.

[18] A. Smith, "High-Lift Aerodynamics," *Journal of Aircraft*, vol. 12, pp. 501–530, 1975.

[19] Y. Wang and G.-C. Zha, "Study of Mach Number Effect for 2D Co-Flow Jet Airfoil at Cruise Conditions." AIAA Paper 2019-3169, AIAA Aviation 2019, AIAA Applied Aerodynamics Conference, Dallas, Texas, 17-21 June 2019.

[20] Y. Wang and G.-C. Zha, "Study of 3D Co-flow Jet Wing Induced Drag and Power Consumption at Cruise Conditions." AIAA Paper 2019-0034, AIAA SciTech 2019, San Diego, CA, January 7-11, 2019.

[21] Y.-Q. Shen and G.-C. Zha, "Large Eddy Simulation Using a New Set of Sixth Order Schemes for Compressible Viscous Terms ," *Journal of Computational Physics*, vol. 229, pp. 8296–8312, 2010.

[22] Zha, G.C., Shen, Y.Q. and Wang, B.Y., "An improved low diffusion E-CUSP upwind scheme ," *Journal of Computer and Fluids*, vol. 48, pp. 214–220, Sep. 2011.

[23] Y.-Q. Shen and G.-Z. Zha , "Generalized finite compact difference scheme for shock/complex flowfield interaction," *Journal of Computational Physics*, vol. doi:10.1016/j.jcp.2011.01.039, 2011.

[24] Shen, Y.-Q. and Zha, G.-C. and Wang, B.-Y., " Improvement of Stability and Accuracy of Implicit WENO Scheme," *AIAA Journal*, vol. 47, No. 2, pp. 331–344, 2009.

[25] Shen, Y.-Q. and Zha, G.-C. and Chen, X.-Y., " High Order Conservative Differencing for Viscous Terms and the Application to Vortex-Induced Vibration Flows," *Journal of Computational Physics*, vol. 228(2), pp. 8283–8300, 2009.

[26] Shen, Y.-Q. and Zha, G.-C. , " Improvement of the WENO Scheme Smoothness Estimator," *International Journal for Numerical Methods in Fluids*, vol. DOI:10.1002/fld.2186, 2009.

[27] G.-C. Zha and E. Bilgen, "Numerical Study of Three-Dimensional Transonic Flows Using Unfactored Upwind-Relaxation Sweeping Algorithm," *Journal of Computational Physics*, vol. 125, pp. 425–433, 1996.

[28] B.-Y. Wang and G.-C. Zha, "A General Sub-Domain Boundary Mapping Procedure For Structured Grid CFD Parallel Computation," *AIAA Journal of Aerospace Computing, Information, and Communication*, vol. 5, No.11, pp. 2084–2091, 2008.

[29] Y.-Q. Shen, G.-C. Zha, and B.-Y. Wang, "Improvement of Stability and Accuracy of Implicit WENO Scheme ," *AIAA Journal*, vol. 47, pp. 331–344, 2009.